

$K_S^0 K\pi$ production in tagged and untagged $\gamma\gamma$ interactions

CELLO Collaboration

H.J. Behrend, L. Criegee, J.B. Dainton¹, J.H. Field²,
G. Franke, H. Jung³, J. Meyer, V. Schröder,
G.G. Winter
Deutsches Elektronen-Synchrotron, DESY, Hamburg,
Federal Republic of Germany

P.J. Bussey, C. Buttar⁴, A.J. Campbell, D. Hendry,
G. McCurrach, J.M. Scarr, I.O. Skillicorn,
K.M. Smith
University of Glasgow, UK

J. Ahme, V. Blobel, W. Brehm, M. Feindt,
H. Fenner, J. Harjes, J.H. Peters, O. Podobrin,
H. Spitzer

II. Institut für Experimentalphysik, Universität, Hamburg,
Federal Republic of Germany

W.-D. Apel, J. Engler, G. Flügge³, D.C. Fries,
J. Fuster⁵, P. Gabriel, K. Gamberdinger⁶,
P. Grosse-Wiesmann⁷, M. Hahn, U. Hädinger,
J. Hansmeyer, J. Knapp, H. Küster⁸, H. Müller,
K.H. Ranitzsch, H. Schneider, R. Seufert, J. Wolf
Kernforschungszentrum Karlsruhe und Universität, Karlsruhe,
Federal Republic of Germany

Received November 1988

Abstract. We have searched for resonance production in the reaction $\gamma\gamma \rightarrow K_S^0 K\pi$. No signal was found for the η_c and an upper limit for the radiative with $\Gamma_{\gamma\gamma}^{\eta_c} < 12$ keV (95% c.l.) is obtained. For the glueball candidate $\eta(1440)$ (previously ι) the upper limit $\Gamma_{\gamma\gamma}^{\eta(1440)} B(\eta(1440) \rightarrow K\bar{K}\pi) < 1.2$ keV (95% c.l.) is derived. In the tagged data sample resonance formation of a spin 1 state at 1420 MeV is observed, which is absent in the untagged data. The mass and width

W. de Boer, G. Buschhorn, G. Grindhammer⁹,
B. Gunderson, Ch. Kiesling¹⁰, R. Kotthaus,
H. Kroha, D. Lüers, H. Oberlack, P. Schacht,
S. Scholz, G. Shooshtari, W. Wiedenmann
Max-Planck-Institut für Physik und Astrophysik, München,
Federal Republic of Germany

M. Davier, J.F. Grivaz, J. Haissinski, P. Janot,
V. Journé, Kim D.W., F. Le Diberder, J.-J. Veillet
Laboratoire de l'Accélérateur Linéaire, Orsay, France

K. Blohm, R. George, M. Goldberg, O. Hamon,
F. Kapusta, L. Poggioli, M. Rivoal
Laboratoire de Physique Nucléaire et Hautes Energies,
Université, Paris, France

G. d'Agostini, F. Ferrarotto, M. Iacovacci, B. Stella
University of Rome and INFN, Rome, Italy

G. Cozzika, Y. Ducros
Centre d'Etudes Nucléaires, Saclay, France

G. Alexander, A. Beck, G. Bella, J. Grunhaus,
A. Klatchko, A. Levy, C. Milstène
Tel Aviv University, Israel

of this state are consistent with those of the $f_1(1420)$; an analysis of decay angular distributions favours positive parity.

1 Introduction

In the reaction $\gamma\gamma \rightarrow K_S^0 K\pi$ several experiments have searched for the formation of the η_c . The $\gamma\gamma$ coupling of the η_c is of theoretical interest since the ratio of the partial $\gamma\gamma$ width to the total hadronic width gives a test of perturbative QCD relating the two gluon to the two photon coupling [1]. The experimental results on $\Gamma_{\gamma\gamma}^{\eta_c}$ obtained so far seem to indicate some discrepancy. The PLUTO collaboration first reported a signal and quoted $\Gamma_{\gamma\gamma}^{\eta_c} = 28 \pm 15$ keV [2]. However, another result [3] and subsequent measurements by other groups could not consistently confirm the PLUTO result and tend to considerably lower values

¹ Permanent address: University of Liverpool, UK

² Now at Université de Geneve, Switzerland

³ Now at RWTH, Aachen, FRG

⁴ Now at Nuclear Physics Laboratory, Oxford, UK

⁵ Now at Inst. de Fisica Corpuscular, Universidad de Valencia, Spain

⁶ Now at MPI für Physik und Astrophysik, München, FRG

⁷ Now at Stanford Linear Accelerator Center, USA

⁸ Now at DESY, Hamburg, FRG

⁹ On leave at Stanford Linear Accelerator Center, USA

¹⁰ Heisenberg Scholarship of Deutsche Forschungsgemeinschaft

of $\Gamma_{\gamma\gamma}^{\eta_c}$ [4–8]. We have studied the reaction $\gamma\gamma \rightarrow K_S^0 K \pi$ to provide additional information on this topic.

The $\eta(1440)$ (previously i) has been observed in the final state $K\bar{K}\pi$ in radiative J/ψ decays [10]. Several $\gamma\gamma$ experiments set upper limits on the radiative width of the $\eta(1440)$, the best limit coming from the TPC/2 γ Collaboration [9]. Its copious production in J/ψ decays, combined with the lack of a clear signal in hadronic experiments, has made the $\eta(1440)$ the most promising glueball candidate. The small two photon coupling of the $\eta(1440)$ supports this interpretation.

The recent observation of a resonance at 1420 MeV decaying into $K_S^0 K \pi$ has attracted much attention [11–13]. Since it is visible only if one of the photons is far off mass shell (denoted below by γ^*) it is concluded that it is a spin 1 state. It is suggestive to identify this state with the $f_1(1420)$ (the former $E(1420)$) and to interpret it as the second isoscalar beside the $f_1(1285)$ (previously $D(1285)$) in the axial vector nonet. While the $f_1(1285)$, which is also seen in $\gamma\gamma^*$ scattering, is a well established 1^{++} state the status of the $f_1(1420)$ observed in hadron reactions is less clear. In some hadron production experiments the $f_1(1420)$ is seen to be $J^P=1^+$ [14] whereas others observe a $J^P=0^-$ state [15]. If the latter is correct the $f_1(1420)$ might have been confused with the $\eta(1440)$, a fact known as the E/i puzzle. In a recent experiment the LASS Collaboration found no evidence for the $f_1(1420)$ in the hypercharge exchange reaction $K^- p \rightarrow K_S^0 K \pi \Lambda$ [16]. Instead they confirmed a 1^{++} state at higher mass, the $f_1(1530)$, which is proposed to be the $s\bar{s}$ rich state f_1' in the 1^{++} nonet. Thus the interpretation of the $f_1(1420)$ in the axial vector nonet is not unambiguous. It has been speculated [17] that several experimental observations might be explained by the existence of a $q\bar{q}g$ hybrid state with exotic quantum numbers $J^{PC}=1^{-+}$. In this paper we present the observation of a resonance in $\gamma\gamma^* \rightarrow K_S^0 K \pi$ at 1420 MeV. Since the identification with the $f_1(1420)$ is not yet clear it is tentatively denoted by $X(1420)$. Beside the measurement of the $\gamma\gamma$ coupling we investigate its decay mode and possible parity assignments.

2 Detector description and data collection

The experiment was performed with the CELLO detector at the PETRA storage ring. The data were collected at a beam energy of 17.5 GeV and correspond to an integrated luminosity of 86 pb $^{-1}$. For the single tag analysis we used in addition a data sample of 9 pb $^{-1}$ taken at a beam energy of 19.1 GeV.

A detailed description of the CELLO detector can be found elsewhere [18]. Here we briefly mention the main components important for the present analysis.

Charged particles are measured in the central detector, which consists of a system of cylindrical drift and proportional chambers. The central detector is surrounded by a thin superconducting coil providing a solenoidal magnetic field of 1.3 T. The angular acceptance is 91% of 4π and a momentum resolution of $\sigma(p)/p=0.02 \cdot p$ (p in GeV/c) without beam constraint is achieved. The tracking system is completed by two planes of proportional chambers perpendicular to the beam in the forward and backward region which allow charged particle measurement within $|\cos\theta| \leq 0.98$.

A 20 radiation lengths deep lead liquid argon calorimeter with fine lateral and longitudinal segmentation is subdivided into two main parts: the barrel covering $|\cos\theta| < 0.86$, and the end caps ranging from $|\cos\theta|=0.92$ to $|\cos\theta|=0.99$. The energy resolution for electromagnetic showers can be parametrized as $\sigma/E = 5\% + 10\%/\sqrt{E}$ (E in GeV). The acceptance gap between barrel and end cap is closed by a lead scintillator sandwich which provides veto capability rather than a precise energy measurement. Hermetic calorimetry down to 50 mrad is completed by forward shower counters consisting of lead glass arrays. Both the end caps and the forward shower counters were used in this analysis for tagging purposes.

For triggering of charged particle final states a microprocessor was used as a fast track finder in the $r\phi$ and rz plane of the central detector [19]. In the untagged analysis we accepted only events with charged triggers because their efficiencies can be cross checked and they can reliably be simulated by applying the same track finding algorithm as used in the trigger to the hit pattern of Monte Carlo events. The basic trigger requirements were at least two charged particles with p_t above 650 MeV/c or two tracks above 250 MeV/c with an opening angle larger than 45° (135° in part of the experiment). For tagged events one track with p_t above 250 MeV/c was sufficient to pass the trigger logic.

3 Event selection

In order to identify events of the type $e^+e^- \rightarrow e^+e^- K_S^0 K \pi$, with $K_S^0 \rightarrow \pi^+\pi^-$, we first selected events with four charged particles and zero net charge. Events with additional neutrals were rejected by demanding that no isolated shower energy above 100 MeV was detected. To identify the K_S^0 by its in flight decay a secondary vertex (V^0) search routine

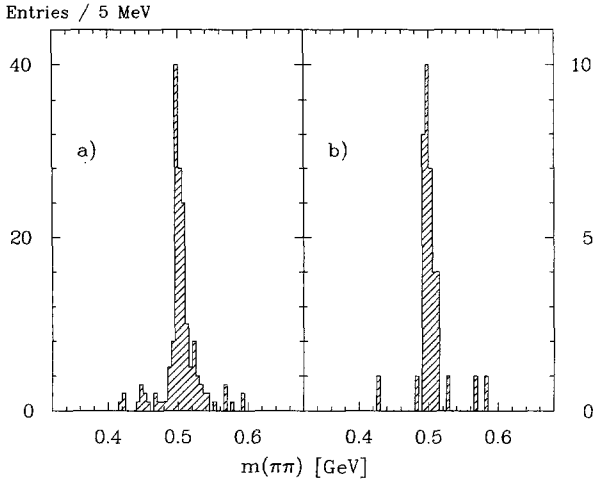


Fig. 1. Invariant $\pi^+ \pi^-$ mass spectrum for secondary vertices in the no tag **a** and single tag **b** sample

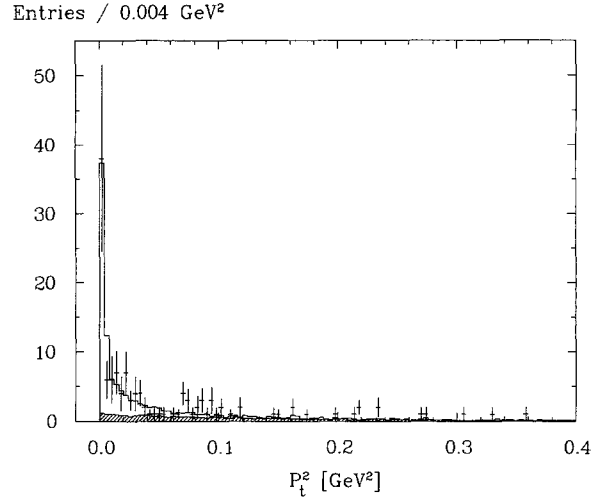


Fig. 2. Distribution of $|\Sigma \mathbf{p}_t|^2$ in the untagged sample; the histogram is the Monte Carlo expectation for exclusive $K_S^0 K \pi$ events plus the estimated nonexclusive background (shaded histogram)

was applied to the remaining events. For each pair of oppositely charged tracks a vertex separation in the $r\phi$ plane was calculated, defined as the distance between the intersection point and the primary vertex projected on the momentum sum of the two particles. The primary vertex was determined from Bhabha events for each run. Candidates with vertex separation less than 4 mm were rejected. Both particles were required to be incompatible with originating from the primary vertex by more than one standard deviation. Furthermore it was demanded that both particles be compatible with originating from a common secondary vertex within a χ^2 of 12. V^0 candidates passing the cuts were then fitted to the secondary vertex hypothesis. Only events with one V^0 and $m_{V^0}(\pi\pi)$ between 0.4 and 0.6 GeV were kept, which is sufficient to determine the background from misidentified K_S^0 .

To suppress potential background from $K_S^0 K_S^0$ events the V^0 search routine was rerun with considerably looser cuts on the tracks recoiling against the K_S^0 candidate. Events in which a second K_S^0 candidate was found were rejected. The remaining $K_S^0 K_S^0$ background was estimated using the measured cross section $\sigma(\gamma\gamma \rightarrow K^0 \bar{K}^0)$ [20] in a Monte Carlo simulation and corresponds to 1.5% in the final sample.

The events were then split into a single tag and an untagged sample by requiring either a tag energy larger than 5 GeV or no shower energy above 1 GeV in the forward or end cap calorimeters. Since the untagged sample showed slightly more background under the K_S^0 an additional cut in the V^0 quality was introduced. The product of the vertex separation in standard deviations and the probability of the secondary vertex fit was required to be larger than 3 in

the untagged sample and larger than 1 for single tag events. In Fig. 1 the resulting V^0 invariant mass distribution is shown. It shows a clear K_S^0 signal above very little background in both samples. For further analysis K_S^0 candidates with V^0 masses between 0.47 GeV and 0.53 GeV were accepted and the K_S^0 mass of 0.498 GeV assigned. After these cuts 129 events remained in the untagged and 35 events in the single tag sample.

4 The untagged data sample

In order to suppress background from events with additional undetected particles the net transverse momentum of the $K_S^0 K \pi$ system was restricted to be $|\Sigma \mathbf{p}_t| < 200$ MeV. The $|\Sigma \mathbf{p}_t|^2$ distribution is shown in Fig. 2.

Figure 3 shows the invariant $K_S^0 K \pi$ mass distribution. The invariant mass was calculated by assigning K and π masses respectively to the tracks recoiling against the K_S^0 yielding two entries per event. There is no resonance-like structure visible and especially in the mass regions of the $\eta(1440)$ and the η_c no enhancements are observed.

For the acceptance calculation concerning the reactions $\gamma\gamma \rightarrow \eta_c$, $\eta(1440) \rightarrow K_S^0 K \pi$ the $\gamma\gamma$ system was generated according to the flux of transverse photons using the exact formula of [23] and a ρ form factor. Breit-Wigner mass distributions were assumed for both resonances with the standard values for mass and width [21] and isotropic phase space for the decay. Furthermore events with a flat distribution of

Entries / 100 MeV

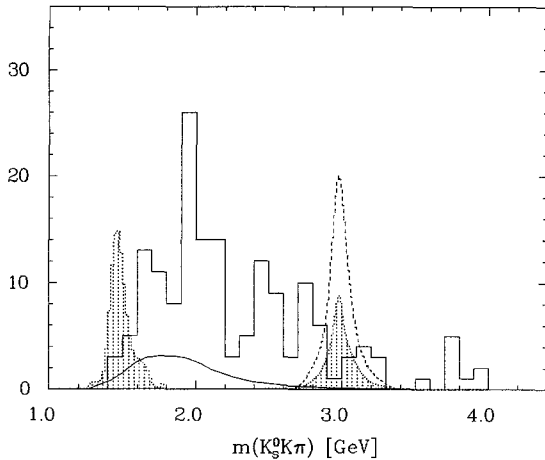


Fig. 3. Invariant $K_S^0 K \pi$ mass distribution with two entries per event. The dashed histogram shows the expectation from the PLUTO result, the dotted histograms correspond to the upper limits $\Gamma_{\gamma\gamma}^{\eta_c} < 12$ keV and $\Gamma_{\gamma\gamma}^{\eta(1440)} \cdot B(\eta(1440) \rightarrow K\bar{K}\pi) < 1.2$ keV. The full line indicates the background

the $\gamma\gamma$ energy $W_{\gamma\gamma}$ were generated in order to determine the $W_{\gamma\gamma}$ dependent reconstruction efficiency. All events were passed through a full detector simulation and through the analysis chain applied to the data. To derive an upper limit for the radiative width of the η_c we define an η_c candidate by requiring that both invariant mass combinations are within 150 MeV around the nominal η_c mass. In the Monte Carlo simulation 85% of the η_c events are retained by this procedure. In the data only one candidate is found which results in the upper limit:

$$\Gamma_{\gamma\gamma}^{\eta_c} \cdot B(\eta_c \rightarrow K_S^0 K \pi) < 0.21 \text{ keV (95\% c.l.)} \quad (1)$$

Using $B(\eta_c \rightarrow K_S^0 \pi) = 1.8\%$ [21] this corresponds to $\Gamma_{\gamma\gamma}^{\eta_c} < 12$ keV, but one should keep in mind that this branching ratio is uncertain by $\pm 0.6\%$. In Table 1 our result for $\Gamma_{\gamma\gamma}^{\eta_c}$ is compared with those of other experiments. There is no significant discrepancy between the experiments taking into account the large uncertainty of the PLUTO value. However, the measurements of $\Gamma_{\gamma\gamma}^{\eta_c}$ as well as the quoted upper limits favour a value well below 10 keV.

We also set an upper limit on the radiative width of the $\eta(1440)$. $\eta(1440)$ candidate events were selected requiring both invariant masses to be within 150 MeV around the nominal $\eta(1440)$ mass. Three candidates are found and attributing these to $\eta(1440)$ production gives an upper limit for the radiative width times branching ratio of:

$$\Gamma_{\gamma\gamma}^{\eta(1440)} \cdot B(\eta(1440) \rightarrow K\bar{K}\pi) < 1.2 \text{ keV (95\% c.l.)} \quad (2)$$

Table 1. Measurements of $\Gamma_{\gamma\gamma}^{\eta_c}$

Experiment	Ref.	$\Gamma_{\gamma\gamma}^{\eta_c}$ (keV)
CELLO		<12 95% c.l.
JADE (prel.)	[6]	<11 95% c.l.
TPC/2 γ	[5]	<15.5 95% c.l. > 1.7 95% c.l.
MD-1 (pred.)	[7]	<11 90% c.l.
PLUTO	[2]	28 \pm 15
TASSO	[8]	19.9 \pm 6.1 \pm 8.6
Mark II	[4]	8 \pm 6
TPC/2 γ	[5]	6.4 $^{+5.9}_{-3.4}$
R704	[3]	4.3 $^{+3.4}_{-3.7} \pm 2.4$

The upper limits given for the η_c and for the $\eta(1440)$ include a 20% systematic error in the acceptance calculation.

The obviously small $\gamma\gamma$ coupling of the $\eta(1440)$ is in contrast to its copious production in radiative J/ψ decays. Chanowitz [22] introduced the quantity “stickiness” S to describe whether a particle state is primarily built of constituent quarks or gluons. S_X is defined as the ratio of $\Gamma(J/\psi \rightarrow \gamma X)$ to $\Gamma(X \rightarrow \gamma\gamma)$ with phase space factors removed. From our result presented above and additional numbers taken from [21] we get (with S_η normalized to 1):

$$S_h : S_{\eta'} : S_{\eta(1440)} = 1 : 4 : > 80. \quad (3)$$

This result could be evidence for a substantial glue content of the $\eta(1440)$, but it should be noted that this argument is not rigorous since also a pure $q\bar{q}$ state can have a vanishing $\gamma\gamma$ width for certain flavour singlet-octet mixings.

In Fig. 4 we present the topological cross section for $\gamma\gamma \rightarrow K^0 K^- \pi^+ (\bar{K}^0 K^+ \pi^-)$ as a function of $W_{\gamma\gamma}$ after background subtraction. A smooth fall-off from 9 nb at $W_{\gamma\gamma} = 2$ GeV to 1 nb at $W_{\gamma\gamma} = 4$ GeV is observed. Indicated are statistical errors only; the systematic error decreases from 25% in the lower mass bins to 15% for $W_{\gamma\gamma} > 2$ GeV. The systematic error is mainly due to uncertainties in the background subtraction and in the acceptance calculation.

As background sources incompletely reconstructed events and contamination due to misidentified K_S^0 were taken into account. From the side bands of the K_S^0 signal the background due to fake K_S^0 was estimated to be 6%. Background due to higher multiplicity final states such as $K_S^0 K_L^0 \pi \pi$ (e.g. via $\phi \pi \pi$ or $K^{*0} \bar{K}^{*0}$) where the K_L^0 escapes undetected was estimated by studying the $|\Sigma \mathbf{p}_i|^2$ (henceforth abbreviated by p_i^2) distribution of the tracks: We fitted the p_i^2

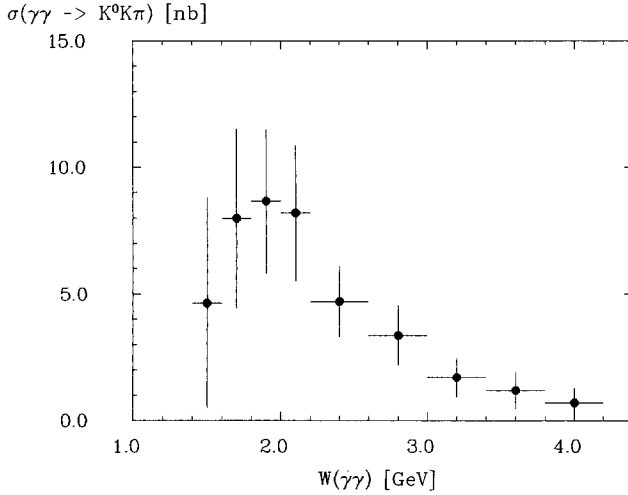


Fig. 4. Topological cross section for the reaction $\gamma\gamma \rightarrow K^0 K^- \pi^+ (\bar{K}^0 K^+ \pi^-)$. The indicated errors are statistical only

spectrum of $K_S^0 K \pi$ Monte Carlo events plus a background contribution to the observed p_i^2 distribution. For the background we tried both a flat behaviour in p_i^2 and the p_i^2 spectrum of higher multiplicity Monte Carlo events. The background was determined in each $W_{\gamma\gamma}$ bin and amounts in total to 10% with a systematic uncertainty of $\pm 4\%$ arising from the different assumptions of the background p_i^2 spectrum.

5 The single tag data sample

In the single tag sample a momentum balance $|\Sigma \mathbf{p}_i| < 450$ MeV, including the tag, was required to reject events with unreconstructed particles or badly measured tags. To suppress background further the sample was visually scanned and events with undetected particles were removed. The final sample contains 29 events.

The invariant $K_S^0 K \pi$ mass distribution is shown in Fig. 5 with two entries per event. A clear signal around 1400 MeV is visible, while in the untagged sample no comparable structure is found, as seen from Fig. 3. Such a signature is expected for a spin 1 particle. Two real, that is massless, and therefore transversely polarized photons cannot couple to a spin 1 object according to Yang's theorem [27]. But no such selection rule applies if one of the photons is highly virtual, and may be tagged by the detection of an outgoing e^\pm at a large scattering angle. A Monte Carlo simulation shows that a spin 0 resonance yielding the observed signal in the tagged data sample would show up with about 150 entries in our untagged data.

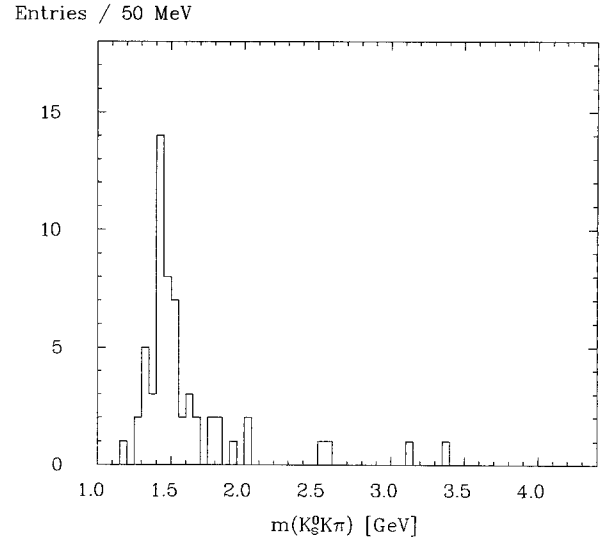


Fig. 5. Invariant $K_S^0 K \pi$ mass distribution for single tag events (2 entries per event)

Only very few events are seen there; thus the spin 1 assignment is evident.

To determine the mass and width of the resonance provisionally denoted X we selected events with at least one entry in the mass range from 1.36 to 1.48 GeV. There are 17 events in this region, the mass distribution of which is given in Fig. 6a). Two independent methods were used to eliminate the twofold ambiguity in the mass assignment of the two unidentified charged particles. Since it will be shown below that the final state is consistent with being pure $\bar{K}^* K (K^* \bar{K})$, in the first method the charged K is chosen by selecting the best K^* candidate in the event. The resulting invariant mass distribution is shown in Fig. 6b). A Breit-Wigner was fitted to the signal using 20 MeV bins and a flat background of 0.2 events per bin. The second method, which is less dependent on the assumed decay mode, uses Monte Carlo events generated with a flat mass distribution. The events were weighted with a Breit-Wigner using for each event the generated mass $W_{\gamma\gamma}$ and as variables the resonance parameters M and Γ in a maximum likelihood fit to the observed mass distribution. The two methods yield consistent values. Our results are:

$$M = 1425 \pm 10 \text{ MeV} \quad (4)$$

$$\Gamma = 42 \pm 22 \text{ MeV}. \quad (5)$$

The error include statistics and systematics. The mass resolution of $\sigma = 15$ MeV, as determined from Monte Carlo, is unfolded.

From the side bands of the signal and by Monte Carlo studies of the reaction $\gamma\gamma^* \rightarrow f_1(1285) \rightarrow K_S^0 K \pi$ the nonresonant background in the signal is estimated

Entries/50 MeV

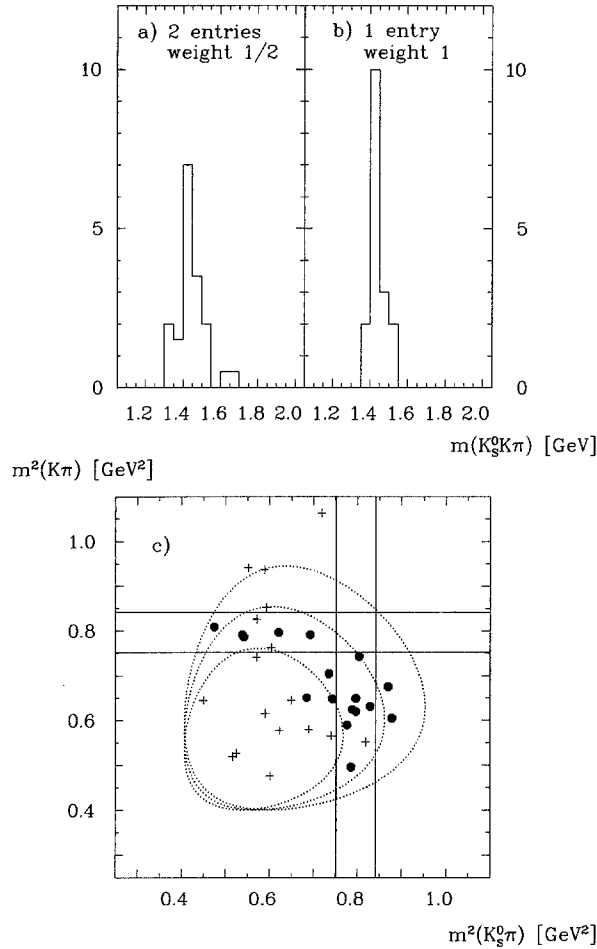


Fig. 6. **a** Invariant masses of the selected signal events; 2 entries are used with weight 1/2. **b** Invariant masses using one entry per event defined by the best K^* candidate. **c** Dalitz plot distribution: The dots denote the selected mass combination corresponding to **b** and the crosses indicate the second possible combination. The dotted lines indicate the kinematic limits for a mass of 1.3, 1.4 and 1.5 GeV

to be 2.2 events. There is room for a few $f_1(1285)$ events in the data and the possible leakage into the $X(1420)$ region was taken into account.

We now turn to the determination of the $\gamma\gamma$ coupling of the state. The total cross section $\sigma(e^+e^- \rightarrow e^+e^-X)$ is related to the $\gamma\gamma$ cross sections σ_{ij} by [23]:

$$\frac{E_1 E_2 d^6 \sigma}{d^3 p_1 d^3 p_2} = \sum_{i,j} \mathcal{L}_{ij} \sigma_{ij} \quad (6)$$

where E_1, E_2, p_1, p_2 are the energies and momenta of the outgoing e^\pm and \mathcal{L}_{ij} are the luminosity functions; the indices i and j denote transverse (T) and longitudinal (L) photon polarizations. In the single tag mode one of the photons is far off mass shell and has transverse and longitudinal polarization

Table 2. Absolute squares of helicity amplitudes

J^P	$ M_{++} ^2$	$ M_{0+} ^2$
1^+	$\frac{(q_2^2 - q_1^2)^2}{W^2} F_{TT0}^2$	$\frac{-q_1^2}{(q_1 \cdot q_2)^2} X F_{LT\text{eff}}^2$
1^-	$\frac{4(q_2^2 - q_1^2)^2}{W^2} X F_{TT0}^2$	$\frac{-q_1^2}{(q_1 \cdot q_2)^2} F_{LT\text{eff}}^2$

states, whereas the other photon is restricted to small virtuality and therefore dominantly to transverse polarization. The formation of a spin 1 state proceeds thus either through collision of one longitudinal and one transverse (LT) or through two transverse (TT) photons. In the first case the spin of the produced state is aligned along the γ momentum axis ($J_z = \pm 1$) in the $\gamma\gamma$ center of mass and in the second the orientation is perpendicular ($J_z = 0$). In a general approach the relevant cross sections can be written in terms of helicity amplitudes following the convention of [24]:

$$\sigma_{TT} = \frac{1}{4\sqrt{X}} \frac{M_R \Gamma}{(W^2 - M_R^2)^2 + \Gamma^2 M_R^2} |M_{++}|^2 \quad (7)$$

$$\sigma_{LT} = \frac{1}{2\sqrt{X}} \frac{M_R \Gamma}{(W^2 - M_R^2)^2 + \Gamma^2 M_R^2} |M_{0+}|^2 \quad (8)$$

where M_R and Γ are the mass and width of the resonance and X is Møller's flux factor $(q_1 \cdot q_2)^2 - q_1^2 q_2^2$, q_i being the photon four vectors. In the following $-q_1^2 = Q^2$ is associated with the virtual photon and $q_2^2 \approx 0$ in the single tag mode. The helicity amplitudes M_{0+} and M_{++} describe the $\gamma\gamma$ coupling of the state. In the limit $q_1^2 \rightarrow 0$ for a spin 1 state they are restricted by gauge invariance and Bose symmetry to vanish as $\sqrt{-q_1^2}$ and $q_2^2 - q_1^2$ respectively. The explicit form of the amplitudes appropriate for $J^P = 1^+$ and $J^P = 1^-$ states is given in Table 2 [24]. The amplitudes contain form factors corresponding to the TT and LT processes F_{TT0} and $F_{LT\text{eff}}$ which have to be determined experimentally. These form factors generally depend on q_1^2, q_2^2 and W^2 and their relative strength is not fixed. A direct determination of both form factors separately using the total cross section alone is therefore not possible but one can give bounds on the allowed values in the $F_{TT0} - F_{LT\text{eff}}$ plane. To disentangle the contributions due to the TT and LT processes the decay angle distributions can be used since the spin orientation of the produced state is different for both cases. Monte Carlo events were generated with the cross sections (7) and (8) and a $\bar{K}^* K + K^* \bar{K}$ intermediate state was assumed for the decay as described

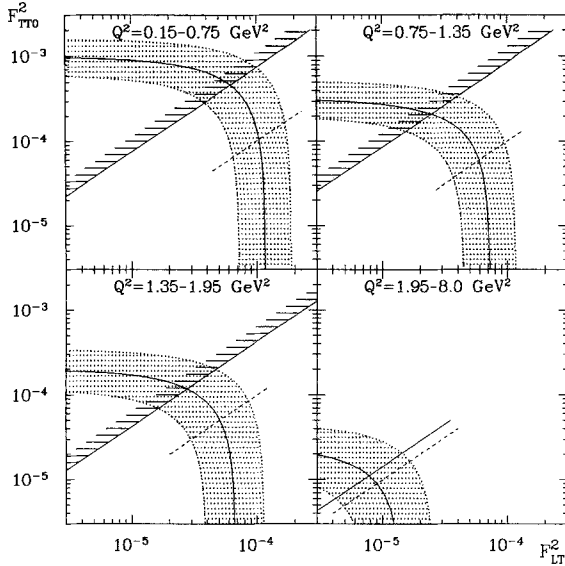


Fig. 7. Allowed (1σ) regions (shaded) for the form factors F_{TT0} and $F_{LT\text{eff}}$ for a $J^P = 1^+$ state. Full lines with horizontal bars indicate regions which are excluded (95% c.l.), full lines without bars indicate values of $F_{TT0}/F_{LT\text{eff}}$ preferred by studies of the decay angle distributions. The dashed lines give $F_{TT0}/F_{LT\text{eff}}$ predicted by Cahn's model

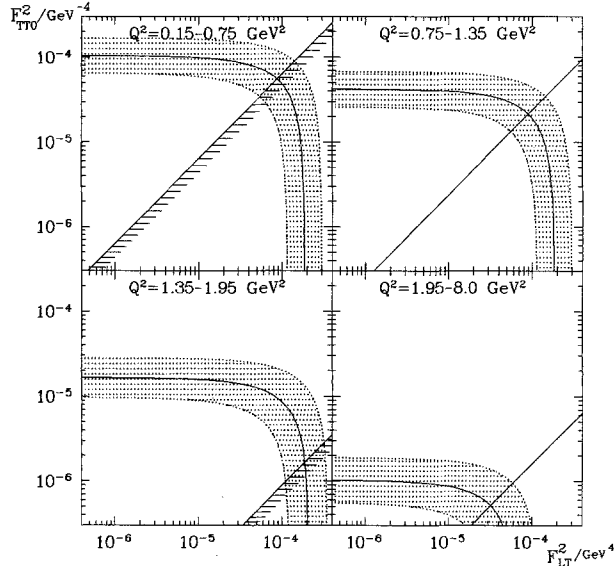


Fig. 8. Allowed regions for the form factors F_{TT0} and $F_{LT\text{eff}}$ for a $J^P = 1^-$ state. Symbols as in Fig. 7

below. The events were passed through the detector simulation and through the analysis chain. In Figs. 7 and 8 we present the allowed regions for the form factors in the $F_{TT0} - F_{LT\text{eff}}$ plane for a $J^P = 1^+$ and for a $J^P = 1^-$ state in four bins of Q^2 . Also indicated are the results of a decay angle analysis either excluding certain regions of $F_{TT0}/F_{LT\text{eff}}$ (95% c.l.) or giving preferred values. However, due to the low statistics

the preferred values have large errors allowing all $F_{TT0}/F_{LT\text{eff}}$ within 1σ . The decay angle analysis will be described in more detail below.

To describe the $\gamma\gamma$ coupling of the spin 1 state by a single coupling constant one needs a model for the LT and TT contributions and their Q^2 dependences. The model of Cahn [26] is based on a nonrelativistic quark model calculation and therefore is applicable to a nonexotic $J^P = 1^+$ meson. The result is given in the narrow width limit $W = M_R$ and we use this approximation throughout in the following. For our definition of the cross sections this model leads to the following expressions for the LT and TT form factors:

$$F_{TT0}^2 = 32\pi(2J+1) \frac{X}{M_R^5} F^2(q_1^2) F^2(q_2^2) \tilde{\Gamma} \quad (9)$$

$$F_{LT\text{eff}}^2 = 32\pi(2J+1) \frac{(q_1 q_2)^2}{M_R^5} F^2(q_1^2) F^2(q_2^2) \tilde{\Gamma} \quad (10)$$

where the $F(q_i^2)$ are vector meson form factors like a ρ or ϕ pole. Note that this model implies $F_{TT0} \approx F_{LT\text{eff}}$ in good approximation in the kinematic region of this analysis. With this Ansatz the coupling strength is described by a single constant $\tilde{\Gamma}$. Originally the result was given by Cahn for the partial widths $\Gamma_{\gamma\gamma^*}^{TT}$ and $\Gamma_{\gamma\gamma^*}^{LT}$:

$$\begin{aligned} \Gamma_{\gamma\gamma^*}^{TT} &= \frac{k^*}{8\pi(2J+1) M_R^2} (|M_{++}|^2 + |M_{--}|^2) \\ &= \frac{8X^{3/2}}{M_R^6} \frac{(q_1^2 - q_2^2)^2}{M_R^4} F^2(q_1^2) F^2(q_2^2) \tilde{\Gamma} \end{aligned} \quad (11)$$

$$\begin{aligned} \Gamma_{\gamma\gamma^*}^{LT} &= \frac{k^*}{8\pi(2J+1) M_R^2} (|M_{0+}|^2 + |M_{0-}|^2) \\ &= \frac{8X^{3/2}}{M_R^6} \frac{-q_1^2}{M_R^2} F^2(q_1^2) F^2(q_2^2) \tilde{\Gamma} \end{aligned} \quad (12)$$

where $k^* = \sqrt{X}/M_R$ is the photon momentum in the $\gamma\gamma$ center of mass. Our definition of $\tilde{\Gamma}$ is in agreement with the one suggested by Cahn and used by the MARK II Collaboration; the corresponding parameter used by TPC/2 γ and JADE has to be multiplied by 2 for comparison with results given in the convention adopted here.

As with the form factors $F_{LT\text{eff}}$ and F_{TT0} , the partial widths $\Gamma_{\gamma\gamma^*}^{TT}$ and $\Gamma_{\gamma\gamma^*}^{LT}$ cannot be separately measured. The measured cross section is sensitive to the combination* $\Gamma_{\gamma\gamma^*}^\sigma \equiv (1 + \sigma_{TT}/\sigma_{LT}) \cdot \Gamma_{\gamma\gamma^*}^{LT} = \Gamma_{\gamma\gamma^*}^{LT} + \frac{1}{2} \Gamma_{\gamma\gamma^*}^{TT}$. We have neglected here the very small ($< 1\%$) difference in the luminosity functions of the LT and TT processes for the kinematic region of this analysis.

* Note that the total $\gamma\gamma^*$ width is $\Gamma_{\gamma\gamma^*} = \Gamma_{\gamma\gamma^*}^{LT} + \Gamma_{\gamma\gamma^*}^{TT}$

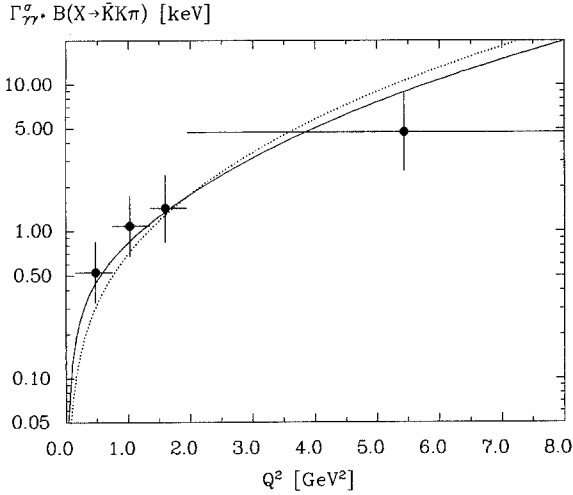


Fig. 9. Q^2 dependence of $\Gamma_{\gamma\gamma}^\sigma \cdot B(X \rightarrow K\bar{K}\pi)$: The full line is the model expectation for the ρ form factor; in the dotted line the ϕ form factor was used

Using the Ansatz (11, 12) $\sigma_{TT}/\sigma_{LT} = Q^2/2M_R^2$ holds in good approximation.

Monte Carlo events were generated with this model assuming either a ρ or a ϕ hole as form factor $F(q_i^2)$ in Eq. (9), (10). Using the ρ form factor the resulting value for $\tilde{\Gamma}$ is:

$$\tilde{\Gamma} \cdot B(X \rightarrow K\bar{K}\pi) = 3.0 \pm 0.9 \pm 0.7 \text{ keV} \quad (13)$$

where the first error is statistical and the second systematic.

In Figure 9 the Q^2 dependence of the width $\Gamma_{\gamma\gamma}^\sigma$ is shown together with the model expectations. The comparison demonstrates that the extracted value of $\tilde{\Gamma}$ does not depend sensitively on the Q^2 range. Restriction to $Q^2 < 2 \text{ GeV}^2$ changes the result to $\tilde{\Gamma} \cdot B(X \rightarrow K\bar{K}\pi) = 3.5 \pm 1.1 \pm 0.8 \text{ keV}$. There is, however, considerable sensitivity to the choice of form factors. Replacing the ρ by a ϕ form factor leaves the acceptance almost unchanged but leads to a lower value of $\tilde{\Gamma}$:

$$\tilde{\Gamma} \cdot B(x \rightarrow K\bar{K}\pi) = 1.4 \pm 0.4 \pm 0.3 \text{ keV}. \quad (14)$$

The corresponding curve for $\Gamma_{\gamma\gamma}^\sigma$ is also indicated in Fig. 9. The values obtained for $\tilde{\Gamma}$ as well as the observed Q^2 dependence are in good agreement with the results of the TPC/2 γ , MARK II and JADE Collaborations [25, 12, 13].

In order to investigate whether the $X(1420)$ can be identified with the $f_1(1420)$ we studied its decay properties and parity by comparing the Dalitz plot with different Monte Carlo expectations. The analysis of a phase space like decay showed that our acceptance is flat over the Dalitz plot variables. Inspection

of the Dalitz plot distribution (see Fig. 6c) indicates an enhancement in the K^* bands. Therefore a $\bar{K}^*K + K^*\bar{K}$ (henceforth abbreviated by K^*K) intermediate state was considered using the matrix element [24] for a K^*K s wave state:

$$M_i = \varepsilon_\beta \left(P_{1i}^\beta \frac{P_{1i} \cdot P_{1-i}}{P_{1i}^2} - P_{1-i}^\beta \right) \frac{1}{P_{1i}^2 - M_{K^*}^2 + i\Gamma_{K^*} M_{K^*}} \quad (15)$$

where $P_{1i} = P_1 + P_i$ and $P_{1-i} = P_1 - P_i$; P_1 is the pion four vector and P_i are the K momenta ($i=2, 3$). ε_β is the polarization vector of the resonance. The interference between the M_i was fixed to be constructive as expected for a C even isoscalar.

We performed a maximum likelihood fit to get a quantitative result on the K^*K contribution. The Dalitz plot was fitted with the expectations for K^*K and for a three body decay. It is found that the data are well described by the above matrix element and require a 90% K^*K contribution with an uncertainty of 25%. This result is consistent with the dominant K^*K decay mode for the $f_1(1420)$ seen in hadronic interactions [14] and in agreement with the observations of the $X(1420)$ in $\gamma\gamma^*$ scattering [25, 12].

The hypothesis of a negative parity exotic $X(1420)$ was also considered. For a negative parity K^*K p wave state ε_β must be replaced by $\varepsilon^\nu \varepsilon_{\mu\nu\gamma\beta} P^\mu P_{1i}^\nu$ in the above formula, P being the four vector of the decaying resonance. In case of $J^P = 1^-$ the Dalitz plot is expected to be depleted near the kinematic boundaries. But this effect is largely compensated in presence of a strong K^*K component. Unlike the $J^P = 1^+$ case there is no model which fixes the ratio σ_{TT}/σ_{LT} for a $J^P = 1^-$ state. Allowing this ratio to vary we obtain reasonably good fits to the Dalitz plot for the $J^P = 1^-$ hypothesis. Thus we are unable to discriminate between the two parity assignments from the Dalitz plot distribution.

Other tests of the parity are possible by studying decay angle distributions. One method has been suggested by Cahn [26]. With θ^* defined as the angle between the normal of the decay plane and the incoming photon in the $\gamma\gamma$ center of mass system, $\cos \theta^*$ is distributed as $1 \pm \cos^2 \theta^*$ for $J^P = 1^\pm$. More precisely this is true for the LT process whereas the respective distributions are $1 - \cos^2 \theta^*$ and $\cos^2 \theta^*$ for the TT part. One gains sensitivity when Q^2 is restricted to small values where the LT process is generally expected to be dominant. We performed a Kolmogorov test for the $\cos \theta^*$ distribution for events with $Q^2 < 1.5 \text{ GeV}^2$ to check the $J^P = 1^\pm$ hypotheses. A probability of 58% is found for the $J^P = 1^+$ hypothesis, to be compared with 9% for $J^P = 1^-$ using σ_{TT}/σ_{LT} according to Cahn's model. It is obvious that this

result strongly depends on σ_{TT}/σ_{LT} . For example setting σ_{TT} to zero gives confidence levels of 71% ($J^P = 1^+$) and 3% ($J^P = 1^-$). On the other hand it should be noted that enhancing σ_{TT} results in higher probabilities for the $J^P = 1^-$ hypothesis. Although general arguments require that σ_{TT}/σ_{LT} vanishes if $Q^2 \rightarrow 0$ the above cut $Q^2 < 1.5 \text{ GeV}^2$ is certainly insufficient to ensure that σ_{TT}/σ_{LT} is necessarily small. Thus we find consistency with the $J^P = 1^+$ hypothesis but a $J^P = 1^-$ state cannot be excluded since there is no sufficient constraint on σ_{TT}/σ_{LT} .

Assuming that the dominant decay mode of the $X(1420)$ is K^*K other angles can be defined to distinguish between s and p wave states ($J^P = 1^+$ and $J^P = 1^-$) and LT and TT ($J_z = \pm 1$ and $J_z = 0$) contributions. The following three angles were chosen for further analysis. θ_{K^*} is defined as the angle between the K^* and the γ axis in the $\gamma\gamma$ center of mass, while the direction of the K from the K^* decay is described by the two angles θ_K and ϕ_K in the K^* center of mass.

The $\cos \theta_{K^*}$ distribution is flat for the s wave LT and TT contributions, whereas it is $1 + \cos^2 \theta_{K^*}$ (LT) and $1 - \cos^2 \theta_{K^*}$ (TT) for the p wave. $\cos \theta_K$ is distributed as $1 - \cos^2 \theta_K$ (LT) s waves and as $1 + \cos^2 \theta_K$ (TT) p waves. The ϕ_K distributions are uniform in all cases except the TTp wave where it varies as $\sin^2 \phi_K$. More distinctive than the projected distributions of these angles are their correlations. In Fig. 10 the $\cos \theta_{K^*} - \cos \theta_K$ correlation as measured in this experiment (a) is compared with Monte Carlo simulations (b–e). We used the angles $\theta_{K^*}, \theta_K, \phi_K$ to obtain results on the relative LT and TT contributions in the four Q^2 bins as mentioned above. In this way combined maximum likelihood fits using the $\theta_{K^*}, \theta_K, \phi_K$ distributions were performed fitting the LT and TT Monte Carlo distributions to the data assuming either $J^P = 1^+$ or $J^P = 1^-$.

In the $J^P = 1^+$ case the results are in the unphysical region of negative TT contributions for the three lower Q^2 bins. Therefore upper limits are given for the TT couplings in figure 7. In the highest Q^2 bin a TT contribution of roughly 50% is favoured, however within the error neither 0% nor 100% can be excluded.

Regarding the $J^P = 1^-$ case the situation is reversed in the sense that strong TT couplings are favoured by the fit throughout. It is worth noting that even in the lowest Q^2 bin ($\langle Q^2 \rangle = 0.5 \text{ GeV}^2$) no LT contribution at all is required, whereas one expects that LT becomes important at low Q^2 since σ_{LT} has to vanish as Q^2 but σ_{TT} as Q^4 . Thus the vanishing or very small LT coupling at low Q^2 is a qualitative argument against the $J^P = 1^-$ hypothesis, unless one

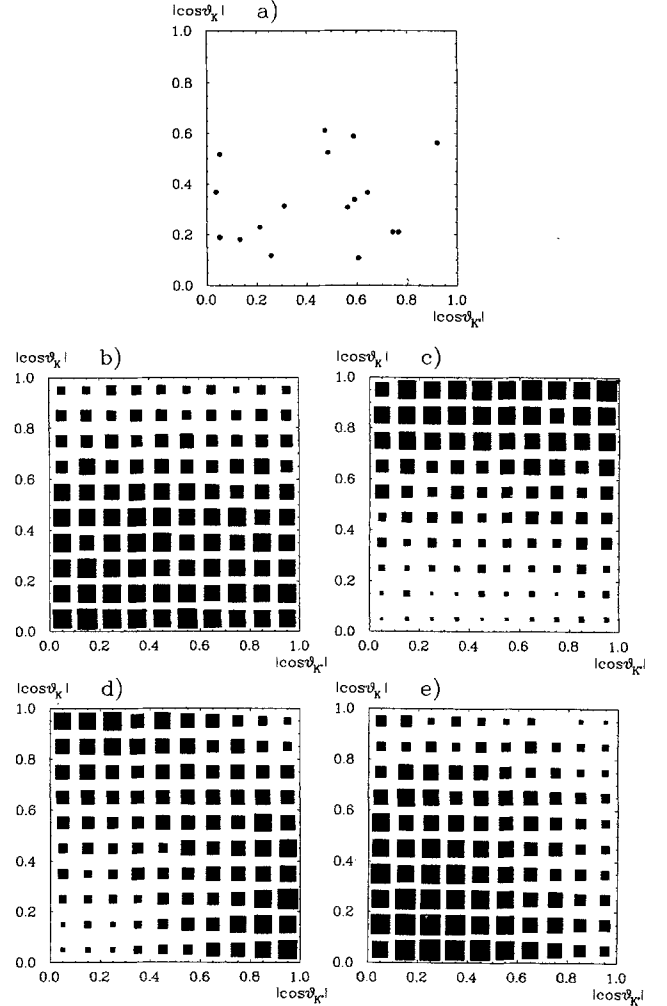


Fig. 10. $|\cos \theta_{K^*}|$ versus $|\cos \theta_K|$: a) Data. b and c: $J^P = 1^+$ LT and TT Monte Carlo. d and e: $J^P = 1^-$ LT and TT Monte Carlo

finds reasons for a dynamical suppression of the LT coupling for an exotic 1^- state. Under this assumption we find that the form factor F_{TT0} is consistent with a ρ pole.

The combined angular distributions were also used to check which J^P hypothesis gives a better description of the data. Using the entire Q^2 range it is found that $J^P = 1^+$ is favoured over $J^P = 1^-$. We also performed Kolmogorov tests for the $\cos \theta_{K^*} - \cos \theta_K$ correlation for the two parity assignments, allowing arbitrary σ_{TT}/σ_{LT} . The highest probability (62%) is found for a $J^P = 1^+$ state with pure LT coupling. For $J^P = 1^-$ the best description is obtained for a state with almost pure TT coupling and has a probability of 36%. Thus we conclude that the distribution of $\cos \theta_{K^*}$ and the combined distributions of $\cos \theta_{K^*}$, $\cos \theta_K$ and ϕ_K favour a $J^P = 1^+$ $X(1420)$, but a $J^P = 1^-$ exotic state with strong TT coupling even at low Q^2 is not ruled out.

6 Summary

We have studied the reaction $\gamma\gamma \rightarrow K_S^0 K \pi$ in the untagged and in the single tag mode. In the untagged data sample no resonant structure is observed and the topological cross section for $\gamma\gamma \rightarrow K^0 K^- \pi^+ (\bar{K}^0 K^+ \pi^-)$ shows a smooth fall-off from 9 nb at $W_{\gamma\gamma}=2$ GeV to 1 nb at $W_{\gamma\gamma}=4$ GeV. From the absence of an η_c signal, an upper limit $\Gamma_{\gamma\gamma}^{\eta_c} \cdot B(\eta_c \rightarrow K_S^0 K \pi) < 0.21$ keV (95% c.l.) is derived. With the branching ratio $B(\eta_c \rightarrow K_S^0 K \pi) = 1.8\%$ the corresponding upper limit $\Gamma_{\gamma\gamma}^{\eta_c} < 12$ keV is obtained. For the glueball candidate $\eta(1440)$ the upper limit $\Gamma_{\gamma\gamma}^{\eta(1440)} \cdot B(\eta(1440) \rightarrow K \bar{K} \pi) < 1.2$ keV (95% c.l.) is derived.

In the single tag reaction $\gamma\gamma^* \rightarrow K_S^0 K \pi$ a resonant state at 1420 MeV, denoted by $X(1420)$, was observed. The fact that this state is not seen in untagged data, i.e. in collisions of almost real photons suggests the $J=1$ assignment. The mass of 1425 ± 10 MeV and the widths of 42 ± 22 MeV are found to be in good agreement with the values of the $f_1(1420)$. Also a dominant K^*K decay mode of the $X(1420)$ is observed consistent with the $f_1(1420)$ seen in hadronic interactions. The $\gamma\gamma$ coupling of the $X(1420)$ was analyzed in terms of the form factors F_{TT0} and $F_{LT\text{eff}}$. Using the nonrelativistic quark model Ansatz of Cahn [26] the $\gamma\gamma$ coupling strength $\tilde{\Gamma}$ has been determined. Assuming a ρ form factor the value $\tilde{\Gamma} = 3.0 \pm 0.9 \pm 0.7$ keV is obtained and $\tilde{\Gamma} = 1.4 \pm 0.4 \pm 0.3$ keV for a ϕ form factor. The analysis of decay angular distributions slightly favours positive parity. Thus all observed properties of the $X(1420)$ are consistent with the $f_1(1420)$, but the hypothesis of an exotic $J^{PC} = 1^{-+}$ hybrid with strong TT coupling is not ruled out.

Acknowledgements. We gratefully acknowledge the outstanding efforts of the PETRA machine group which made possible these measurements. We are indebted to the DESY computer center for their excellent support during the experiment. We acknowledge the invaluable effort of many engineers and technicians from the collaborating institutions in the construction and maintenance of the apparatus. The visiting groups wish to thank the DESY Directorate for

the support and kind hospitality extended to them. This work was partly supported by the Bundesministerium für Forschung und Technologie (FRG), by the Commissariat à l'Energie Atomique and the Institut National de Physique Nucléaire et de Physique des Particules (France), by the Istituto Nazionale di Fisica Nucleare (Italy), by the Science and Engineering Research Council (UK) and by the Ministry of Science and Development (Israel).

References

1. S. Brodsky, P. Lepage: Phys. Rev. D28 (1983) 228; R. Barbieri et al.: Nucl. Phys. B154 (1979) 535; K. Hagiwara, C. Kim, T. Yoshino: B177 (1981) 461
2. PLUTO Coll. Ch. Berger et al.: Phys. Lett. 167B (1986) 120
3. C. Baglin et al.: Proc. Int. Europhysics Conf. on High Energies, Bari, 1985; Phys. Lett. 187B (1987) 191
4. MARK II Coll. Presented by G. Gidal: Proc. 23rd Int. Conf. on High Energy Physics, Berkeley, 1986
5. TPC/2 γ Coll. H. Aihara et al.: Phys. Rev. Lett. 60 (1988) 2355
6. JADE Coll. presented by P. Hill: Proc. Int. Europhysics Conf. on High Energies, Uppsala, 1987
7. A. Blinov et al.: Novosibirsk preprint 86-107, 1986
8. TASSO Coll. W. Braunschweig et al.: DESY 88-050
9. TPC/2 γ Coll. H. Aihara et al.: Phys. Rev. Lett. 57 (1986) 51
10. D. Scharre et al.: Phys. Lett. B97 (1980) 329; C. Edwards et al.: Phys. Rev. Lett. 49 (1982) 259; J. Richman: Ph.D. thesis, California Institute of Technology, 1985; J.E. Augustin et al.: preprint LAL 85/27, 1985
11. TPC/2 γ Coll. H. Aihara et al.: Phys. Rev. Lett. 57 (1986) 2500
12. MARK II Coll. G. Gidal et al.: Phys. Rev. Lett. 59 (1988) 2016
13. JADE Coll. P. Hill et al.: DESY 88-166, subm. for publ. in Z. Phys. C
14. C. Dionisi et al.: Nucl. Phys. B169 (1980) 1; T.A. Armstrong et al.: Z. Phys. C - Particles and Fields 34 (1987) 23
15. P. Baillon et al.: Nuovo Cimento 50A (1967) 393; S.U. Chung et al.: Phys. Rev. Lett. 55 (1985) 779; A. Ando et al.: Phys. Rev. Lett. 57 (1986) 1296
16. LASS Coll. D. Aston et al.: Phys. Lett. 201 (1988) 573
17. M.S. Chanowitz: Phys. Lett. 187B (1987) 409
18. H.J. Behrend et al.: Phys. Scr. 23 (1981) 610
19. H.J. Behrend: Comput. Physics Commun. 22 (1981) 365
20. CELLO Coll. presented by J.H. Peters: Proc. Int. Europhysics Conf. on High Energies, Uppsala, 1987
21. Particle Data Group: Phys. Lett. 170B (1986)
22. M.S. Chanowitz: Proc. Vth International Workshop on Photon-Photon Collisions, Granlibakken, Lake Tahoe 1985, p 95
23. V.M. Budnev et al.: Phys. Rep. 15 (1986) 181
24. M. Poppe: Int. J. Mod. Phys. 1 (1986) 545
25. TPC/2 γ Coll. H. Aihara et al.: Phys. Rev. D38 (1988) 1
26. R.N. Cahn: Phys. Rev. D35 (1987) 3342
27. C.N. Yang: Phys. Rev. 77 (1950) 242